JOURNAL OF MATERIALS SCIENCE 26 (1991) 4567–4580

Analysis of coating interlayer between silicon nitride cutting tools and titanium carbide and titanium nitride coatings

D. G. BHAT*, H. E. REBENNE‡, C. STRANDBERG*
*GTE Valenite Corp., 1711 Thunderbird Street, Troy, MI 48084, USA
‡GTE Laboratories Incorporated, 40 Sylvan Road, Waltham, MA 02254, USA

Silicon nitride (Si_3N_4) cutting tools exhibit excellent thermal stability and wear resistance in the high-speed machining of cast irons, but show poor chemical wear resistance in the machining of steel. Conventional chemical vapour deposition (CVD) coating of Si_3N_4 tools has not been very successful because of thermal expansion mismatch between coatings and the substrate. This problem was overcome by developing a CVD process to tailor the interface for titanium carbide (TiC) and titanium nitride (TiN) coatings. Computer modelling of the CVD process was done to predict which phases would form at the interface, and the results compared with analyses of the interface. Three Si_3N_4 compositions were considered, including pure Si_3N_4, Si_3N_4 with a glass phase binder, and Si_3N_4 + TiC composite with a glass phase binder. Results of machining tests on coated tools show that the formation of an interlayer provides superior wear resistance and tool life in the machining of steel as compared to uncoated and conventionally coated Si_3N_4 tools.

1. Introduction

Advances in the high-speed machining of cast irons in the last few years have become possible due to the use of Si_3N_4-based cutting tools which exhibit high thermal and mechanical stability, hardness, and wear resistance at high machining speeds. Compared to the other ceramic cutting tools in common use, such as alumina (Al_2O_3) and alumina + titanium carbide (Al_2O_3 + TiC) composite, Si_3N_4 has a higher level of fracture toughness and thermal shock resistance [1–4]. This unique combination of properties has made it routinely possible to machine cast irons with Si_3N_4 cutting tools at surface speeds in excess of 1200 m min^{-1} in milling and turning applications [4].

Attempts to use Si_3N_4 tools for machining steel have been largely unsuccessful because of the formation of long, continuous chips which, in contact with the tool at high temperature and ambient atmosphere, cause a rapid chemical reaction with iron. This results in the chemical wear of the insert, which leads to failure by cratering [2]. This problem is not encountered with cast irons which form short chips and, therefore, exhibit minimal chemical wear.

Conventional CVD wear-resistant coatings have been applied to Si_3N_4-based cutting tools [5–8]. For example, Furukawa *et al.* [5] deposited CVD TiN and Al_2O_3 coatings on hot-pressed Si_3N_4 (HPSN) cutting tools. However, they found that use of these tools was limited to the machining of cast irons. Sarin and co-workers [6–8] deposited TiC, TiN, Ti(C,N), and Al_2O_3 coatings on conventional Si_3N_4 cutting tools, as well as on Si_3N_4-based tools containing dispersed second-phase particles of refractory carbides, carbonitrides, or nitrides [7, 8]. They reported some improvements in tool life when machining cast irons and steels.

Improvements in the wear resistance are generally realized when a suitable coating is applied to cutting tools. In the case of composite Si_3N_4 tools, it is found that the second-phase particles of TiC usually act as nucleation sites for the coatings, and provide the necessary diffusion bond for good adhesion. In the absence of a suitable bond, the coating does not adhere well, as illustrated in Fig. 1 where the TiC coating deposited on HPSN shows spontaneous spalling and cracking in the as-coated condition.

An excellent review of the factors affecting adhesion of coatings was published by Steinmann *et al.* [9]. It identified several important factors: surface finish, substrate hardness, coating thickness, loading rate on the coating, and rate of scratching in the scratch-test type of adhesion test. In addition, the nature of chemical bonding between the coating and the substrate, internal stress in the coating, and the nature and magnitude of thermal stresses at the coating–substrate interface will influence adhesion.

For a 5 μm-thick TiC coating deposited at 1298 K on a Si_3N_4-based tool containing 3.5 wt % MgO binder, the room-temperature tangential stress in the coating is about 2.3 GPa (tensile) (see Appendix). This will give rise to a normal compressive stress at the cutting edge of about 0.23 GPa for an edge radius of 50 μm. The corresponding values for TiN are 1.2 and 0.12 GPa, respectively. During machining operations,

0022–2461/91 $03.00 + .12

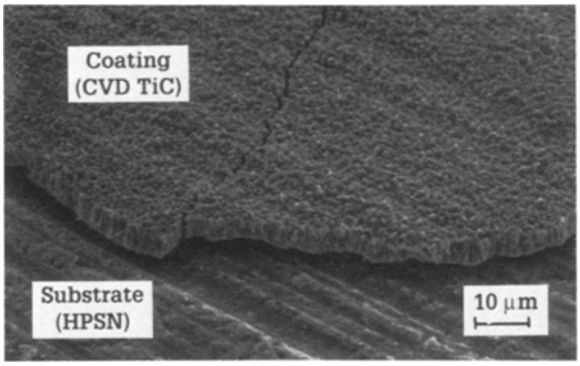

Figure 1 SEM photograph of TiC-coated HPSN showing poor adhesion.

additional stresses are applied to the cutting edge which create further problems for coating adhesion. Under these circumstances, it is necessary to consider methods to improve coating adhesion.

A study was, therefore, undertaken to develop a method of tailoring the interface composition through processing such that interfacial stresses would be minimized. The basic principle of the approach was described earlier [10, 11]. Essentially, it was shown that interaction between Si_3N_4 and $TiCl_4$ vapour at high temperature causes the formation of a surface film of TiN on the substrate according to the following overall reaction:

$$Si_3N_{4(s)} + 4TiCl_{4(g)} + 2H_{2(g)} \rightarrow 4TiN_{(s)} + 3SiCl_{4(g)} + 4HCl_{(g)} \quad (1)$$

The nature of interaction of $TiCl_4$ with the substrate, and the exact composition of the film thus formed, depends on several factors. In this paper, an equilibrium thermodynamic study of this system is presented for different Si_3N_4-based substrates. Comparisons are made between model predictions and compositional and phase analyses of the surfaces of tools. It is shown that a film of TiN forms at the interface, and that this film improves the overall coating adhesion as demonstrated in improved performance during steel machining.

2. Experimental procedure

2.1. Materials

In this study, three Si_3N_4 compositions were considered: CVD α-Si_3N_4 (CVD-SN), hot-pressed Si_3N_4 with a glass phase binder (HPSN), and a composite hot-pressed Si_3N_4 + TiC (HPSNT). The compositions of these are given in Table I.

2.2. Thermodynamic modelling

To assist in interpretation of the experimental results, a thermodynamic analysis of the process was done. The equilibrium composition of a hypothetical system consisting of the substrate and a gas phase containing the species used in the CVD process was calculated for a range of temperatures at atmospheric pressure. The gas-phase composition was varied from 2.2×10^{-4} to 4.4×10^{-2} volume fraction $TiCl_4$ with the H_2 volume fraction held constant at 2.2×10^{-1} and the Ar volume fraction constituting the balance. These values were chosen to give $H_2/TiCl_4$ ratios in the initial gas mixture ranging from 1000 to 5. The substrate compositions are given in Table I. The relative amounts of gas phase and substrate in the initial mixture were 1:1 for all cases. A temperature range of 1323 to 1523 K was used in the calculations. For each case, equilibrium compositions were calculated by minimizing the Gibbs free energy of the system subject to mass balance constraints. This model assumes that every condensed phase is a pure phase; i.e., solid-solution formation is not considered. Calculations were done using a modified NASA chemical equilibrium computer code [12].

2.3. Deposition of coatings

Samples of CVD-SN, HPSN and HPSNT were treated in a gas mixture of $TiCl_4 + H_2 + Ar$ to form the interlayer. Two sets of deposition parameters were used: (i) pressure = 1 atm, temperature = 1423 K, H_2 = 22 vol %, Ar = 73.6 vol %, $H_2/TiCl_4$ ratio = 5, total flow = 100 slpm, time = 1 h; (ii) same as (i) with $H_2/TiCl_4$ ratio = 100 and Ar = 77.8 vol %. Samples of HPSN and HPSNT from the batch treated at $H_2/TiCl_4$ ratio = 5, along with uncoated HPSN and HPSNT samples, were subsequently coated with TiN, TiC, and TiC + Al_2O_3 using standard coating procedures.

2.4. Characterization

The coated samples were characterized by various techniques. The phases present after the interlayer

TABLE I Chemical compositions of substrate materials

Component	Substrate composition					
	CVD-SN		HPSN		HPSNT	
	(wt %)	(mol %)	(wt %)	(mol %)	(wt %)	(mol %)
Si_3N_4	100.0	100.0	92.5	93.0	56.1	70.5
Y_2O_3	0.0	0.0	3.5	5.6	3.7	7.5
Al_2O_3	0.0	0.0	0.5	0.4	1.2	1.1
TiC	0.0	0.0	0.0	0.0	39.0	20.9
MgO	0.0	0.0	3.5	1.0	0.0	0.0

treatment were identified by X-ray diffraction (XRD) using a Scintag Pad V X-ray diffractometer and an FeK_α radiation source ($\lambda = 0.193604$ nm). Depth profiles of the various elements were obtained by scanning Auger microprobe using a Perkin-Elmer PHI 600 scanning Auger multiprobe (SAM). All depth profiles were obtained using a 10 keV, 50 nA electron beam at a spectral resolution of 0.6%. The electron beam was rastered over an approximately 25 μm by 25 μm area. Sputtering was performed with a focused 4 kV Ar^+ ion beam rastered over a 3 mm by 3 mm area. The ion beam was adjusted to provide a sputtering rate of 10 nm min^{-1} in Ta_2O_5. Samples were also examined by scanning electron microscopy (SEM) using a Jeol scanning electron microscope JSM-840A.

2.5. Machining tests

Steel turning tests were used to evaluate the machining performance of coated HPSN and HPSNT tools with and without the interlayer. The test parameters are given in Table II. Machining tests were not performed on CVD-SN since this material is not used in cutting tools. After testing, the inserts were evaluated with a toolmaker's microscope for flank and nose wear, crater formation, and spalling of the coating(s). Selected corners were also examined by SEM.

TABLE II Parameters used for steel turning tests

Work material	AISI 4340 steel
Heat treatment	Quenched and tempered
Hardness	HB 290–310
Tool materials	HPSN and HPSNT
Geometry	SNG 12 04 12 (SNG 433)
Edge preparation	0.20 mm × 20°
Cutting parameters	152 and 213 m min^{-1}
	0.127 mm depth of cut (DOC)
	0.25 mm rev^{-1} feed rate
	15° lead angle
End-point of test	0.38 mm flank or nose wear
	or 0.13 mm crater wear

3. Results and discussion

3.1. Thermodynamic modelling

Initially, the case of a pure Si_3N_4 substrate (e.g. CVD-SN) was evaluated. The results from this case predict that TiN will always form when Si_3N_4 is exposed to $TiCl_4$ and H_2 in the range of conditions considered. When the initial ratio $H_2/TiCl_4$ is large ($\geqslant 1000$), free silicon is also predicted to form (see Table III). The implication of these results for the case of depositing a TiC or TiN coating on an Si_3N_4 substrate using $TiCl_4$ as a source material is that a TiN layer should form on the substrate surface during the early stages of deposition. Furthermore, since the nitrogen for TiN formation must be supplied by the substrate, this layer can only form until the interface between the gas phase and the interlayer becomes depleted of nitrogen. The model predicts that no Ti metal or Ti_xSi_y compounds will form at equilibrium.

The addition of oxides to Si_3N_4, represented by HPSN, gives similar results except that the extent of conversion of $TiCl_4$ to TiN increases. This occurs via the formation of Si_2N_2O, which releases nitrogen to react with the $TiCl_x$ compounds. Reactions are also predicted to occur between the various phases present in the substrate and between these and the gas phase species. For example, AlN is predicted to form from the Al_2O_3 and Si_3N_4 in HPSN. The MgO component of HPSN is stable at high initial ratios $H_2/TiCl_4$, but reacts to form volatile $MgCl_x$ compounds at lower ratios. When the gas phase contains a relatively large amount of Cl_2 (e.g. low initial ratios $H_2/TiCl_4$), YOCl and $YCl_{3(l)}$ form from the Y_2O_3 initially present in HPSN. No Ti metal, Ti_xSi_y, or Ti_xO_z compounds are predicted to form.

When TiC is also present in the substrate, represented by HPSNT, the model predicts that, at equilibrium, all of the TiC is converted to TiN. In practice, this suggests that a TiN layer will form on the surface of each TiC grain that is exposed to the CVD gas mixture, with titanium being provided by the substrate. Similar reactions are predicted to occur

TABLE III Phases predicted by model to be present at equilibrium*

Initial ratio $H_2/TiCl_4$	Substrate		
	CVD-SN	HPSN	HPSNT
1000	Gas, Si, Si_3N_4, TiN	Gas, AlN, MgO, Si_2N_2O, Si_3N_4, TiN, Y_2O_3	Gas, AlN, C, SiC, Si_2N_2O, Si_3N_4, TiN, YOCl, Y_2O_3
100	Same as 1000/1 case	Same as 1000/1 case	Same as 1000/1 case
50	Same as 1000/1 case	Gas, AlN, Si_2N_2O, Si_3N_4, TiN, Y_2O_3	Same as 1000/1 case
10	Gas, Si_3N_4, TiN	Gas, AlN, Si_2N_2O, Si_3N_4, TiN, YOCl, Y_2O_3	Same as 1000/1 case
5	Same as 10/1 case	Gas, AlN, Si_2N_2O, Si_3N_4, TiN, $YCl_{3(l)}$, YOCl	Gas, AlN, C, SiC, Si_2N_2O, Si_3N_4, TiN, $YCl_{3(l)}$, YOCl

*The term "gas" refers to the gas phase, and the subscript "l" denotes liquid phase. All other phases are solid.

with the oxide additives as in HPSN. In addition, free carbon and SiC are predicted to form from the carbon that is released when the titanium in TiC reacts to form TiN. As with the other substrates, no Ti metal, Ti_xSi_y, or Ti_xO_z compounds are predicted to form.

The yield of TiN from $TiCl_4$ was also calculated. The dependence of yield on the initial $TiCl_4/Si_3N_4$ ratio (Ti/N = four times the ratio of $TiCl_4/Si_3N_4$ in the starting material) is shown in Fig. 2 for each of the substrates studied. For very low Ti/N ratios ($< 10^{-3}$), all of the $TiCl_4$ is converted to TiN regardless of the composition of the substrate. At higher Ti/N ratios, the presence of oxides is necessary to maintain complete conversion. As discussed above, high yield at high Ti/N ratios coincides with the formation of Si_2N_2O, which releases nitrogen to react with titanium. The results in Fig. 2 are for a temperature of 1423 K, but similar results are obtained at all temperatures considered. For example, for CVD-SN substrate and a Ti/N value of 0.175, the conversion at 1323 K is 0.8229 while that at 1523 K is 0.8322.

For each of the substrates considered, the model predicts that the surface will be depleted of Si_3N_4. The calculated extent of depletion is inversely proportional to the amount of Si_3N_4 present in the starting material. This indicates that the presence of substrate additives reduces the stability of Si_3N_4. When oxide additives are present, some of the Si_3N_4 is oxidized to Si_2N_2O (see Table III). Fig. 3 shows the stability of Si_3N_4 as a function of the amount of Si_3N_4 initially present in the substrate for a temperature of 1423 K. The influence of gas-phase composition on Si_3N_4 stability is also shown. As with the results in Fig. 2, those in Fig. 3 are nearly independent of temperature. For example, for HPSN at an initial $H_2/TiCl_4$ ratio of 100, the stability of Si_3N_4 ranges from 0.9875 at 1323 K to 0.9854 at 1523 K. For the same conditions, the values for HPSNT are 0.8879 and 0.8680, respectively. All of the converted Si_3N_4 becomes either Si_2N_2O or a gaseous Si_xH_y, Si_xCl_z or $Si_xH_yCl_z$ species.

The results of the thermodynamic analysis indicate that the driving force for formation of a TiN layer on Si_3N_4 is very high. Furthermore, this driving force

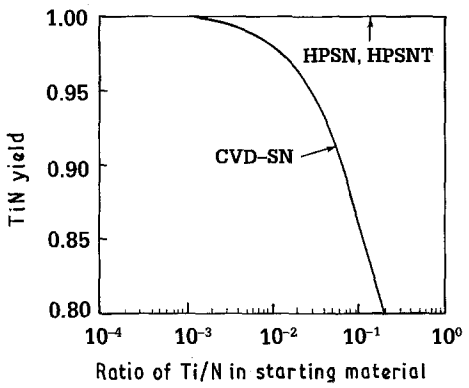

Figure 2 Dependence of TiN yield from $TiCl_4$ on the Ti/N ratio in the starting material. Results are from model predictions at 1423 K. Yield is defined as the number of moles of TiN present at equilibrium divided by the number of moles of $TiCl_4$ initially present. The Ti/N ratio is four times the ratio $TiCl_4/Si_3N_4$ in the starting material.

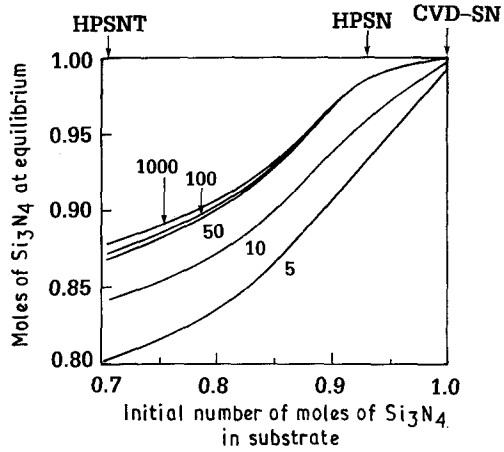

Figure 3 Dependence of stability of Si_3N_4 on the amount of Si_3N_4 present in the starting material. Results are from model predictions at 1423 K. Stability is defined as the number of moles of Si_3N_4 present at equilibrium divided by the number of moles of Si_3N_4 initially present. The labels on the curves denote the ratio $H_2/TiCl_4$ in the initial gas mixture.

increases when oxides or TiC are added to the substrate. In the case of oxide additives, the Si_3N_4 is oxidized to Si_2N_2O, and this releases nitrogen for TiN formation. In the case of TiC additives, the TiC is converted to TiN and carbon-containing gaseous species, and this provides additional titanium for TiN formation. Calculations were also done for lower temperatures, and they gave the same qualitative results. This implies that, in practice, a TiN layer should be present on the surface of any of the substrate materials considered in this work after exposing the substrate to $TiCl_4 + H_2$ at typical CVD temperatures. In addition, the extent of TiN formation should be less on CVD-SN than on the other substrates.

3.2. Characterization

3.2.1. XRD analysis

Samples of CVD-SN, HPSN and HPSNT were examined by XRD to determine the nature of the surface after the interlayer treatment. The XRD spectra are shown in Fig. 4. Fig. 4a shows the spectrum for interlayer-coated CVD-SN. Positions of the TiN peaks are indicated. These are distinct TiN peaks, and there is no overlap of α-Si_3N_4 peaks at these Bragg positions. Similarly, Fig. 4b shows the TiN peaks in the spectrum of interlayer-coated HPSN. Fig. 4c and d show the spectra for HPSNT. As indicated in Table I, this material contains a large amount of TiC which is uniformly distributed in the matrix of Si_3N_4. Fig. 4c shows that the peaks obtained from the sample do not exactly match those of TiN or TiC. This is illustrated in more detail in Fig. 4d, where the sample peak at $2\theta = 54°$ is enlarged. This peak is attributed to Ti(C, N).

These XRD results show clearly that the interlayer reaction gives rise to a TiN film on the surface of Si_3N_4, irrespective of the presence or absence of a glassy grain-boundary phase in the substrate. The XRD data do not show any indication of the presence of (Ti + Si)-type phases. These results are in agreement with the predictions of the thermodynamic model, and with the observations made in a previous study [10].

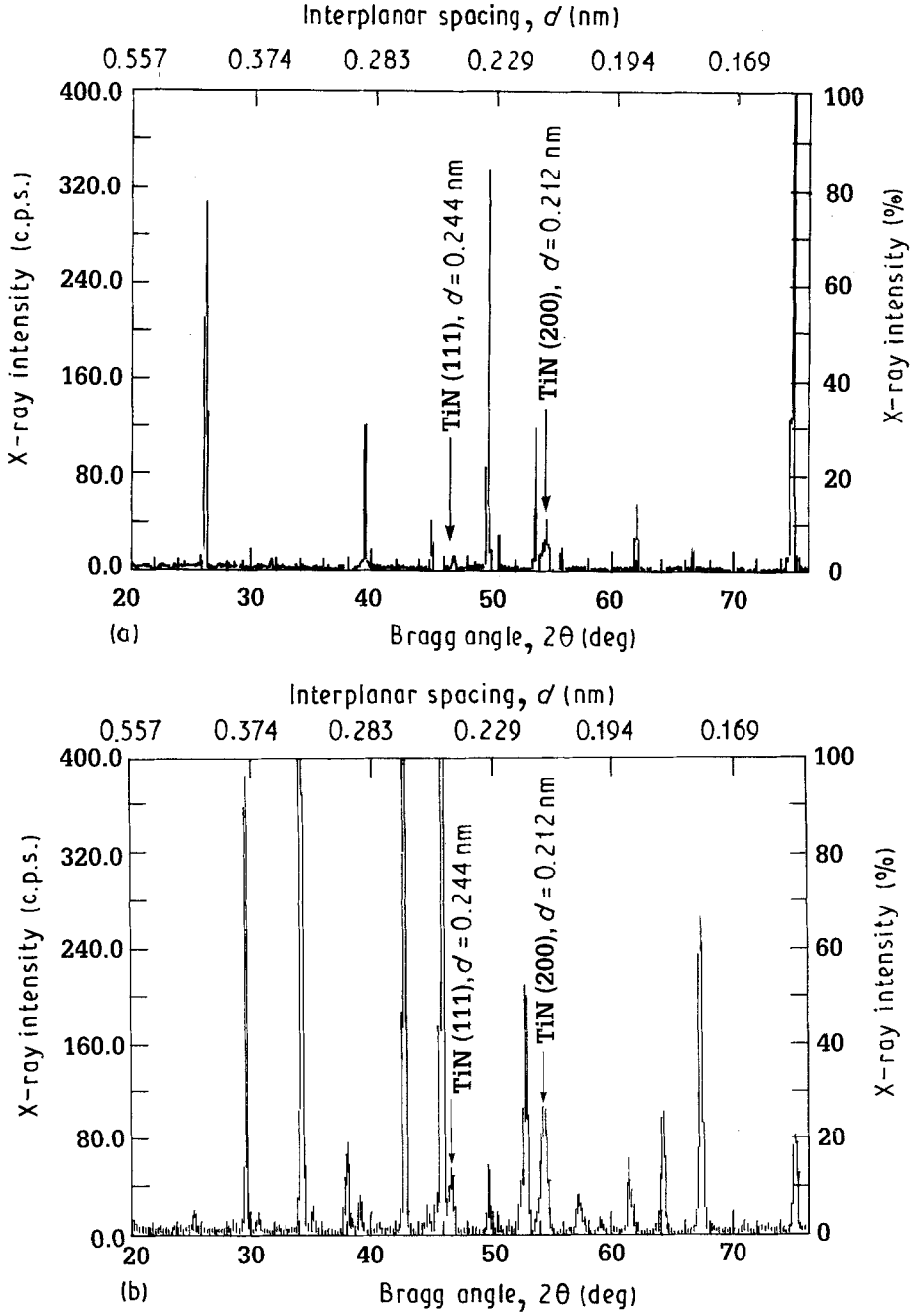

Figure 4 X-ray diffraction spectra for interlayer-coated Si_3N_4 substrates: (a) CVD-SN, (b) HPSN, (c) HPSNT, (d) HPSNT, showing the Ti(C,N) peak at $2\theta = 54°$. FeK_α radiation ($\lambda = 0.193604$ nm) was used to obtain the spectra.

3.2.2. Auger analysis

Results of the SAM analyses are illustrated in Figs 5 and 6 for interlayer-coated CVD-SN and HPSN, respectively. For each substrate, depth profiles obtained on samples treated with $H_2/TiCl_4$ ratios of 5 and 100 are shown.

Fig. 5a shows the data for the case of $H_2/TiCl_4 = 5$ on CVD-SN. A very thin interlayer film is present on the surface (approximately 0.15 μm). The outer 0.06 μm contains Ti, C, N and O. The remainder appears to be TiN. A small amount of Si is present in the interlayer, but the total amount is estimated to be < 30 at %. Fig. 5b shows the data for the case of $H_2/TiCl_4 = 100$. For this case, the interlayer thickness is approximately 1.2 μm, and its structure and composition are different from that in the $H_2/TiCl_4 = 5$ case. A thin layer of TiN (≈ 0.25 μm) is present adjacent to the substrate. In addition, a $Ti_xSi_yN_z$ layer exists in the outer 0.96 μm. The Ti/N ratio in this layer is essentially constant at 3.3, with the amount of Si decreasing in going from the TiN layer to the surface. For example, the composition of the layer ranges from $Ti_5Si_3N_{1.5}$ at a depth of 0.96 μm, to $Ti_5Si_{2.2}N_{1.4}$ at a depth of 0.48 μm, to $Ti_5Si_{1.7}N_{1.5}$ at a depth of 0.24 μm. The $Ti_xSi_yN_z$ layer is believed to be amorphous or extremely fine-grained as no diffraction patterns for $Ti_xSi_yN_z$ compounds could be found by XRD (see above). Finally, a thin layer containing Ti, C, N and O is present at the surface.

For the HPSN sample treated at $H_2/TiCl_4 = 5$ (see Fig. 6a), the total interlayer thickness is five times that on the corresponding CVD-SN sample (e.g. 0.70 μm). This indicates a higher reaction rate between the CVD gas mixture and the substrate. As in the CVD-SN sample prepared at $H_2/TiCl_4 = 100$ (see above), a $Ti_xSi_yN_z$ layer is present, with the level of Si decreasing

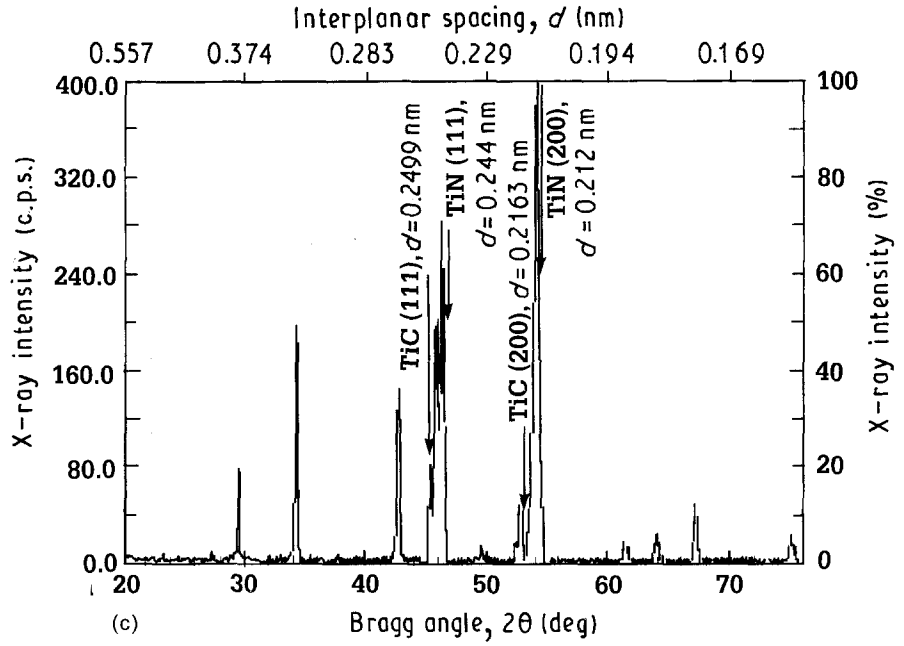

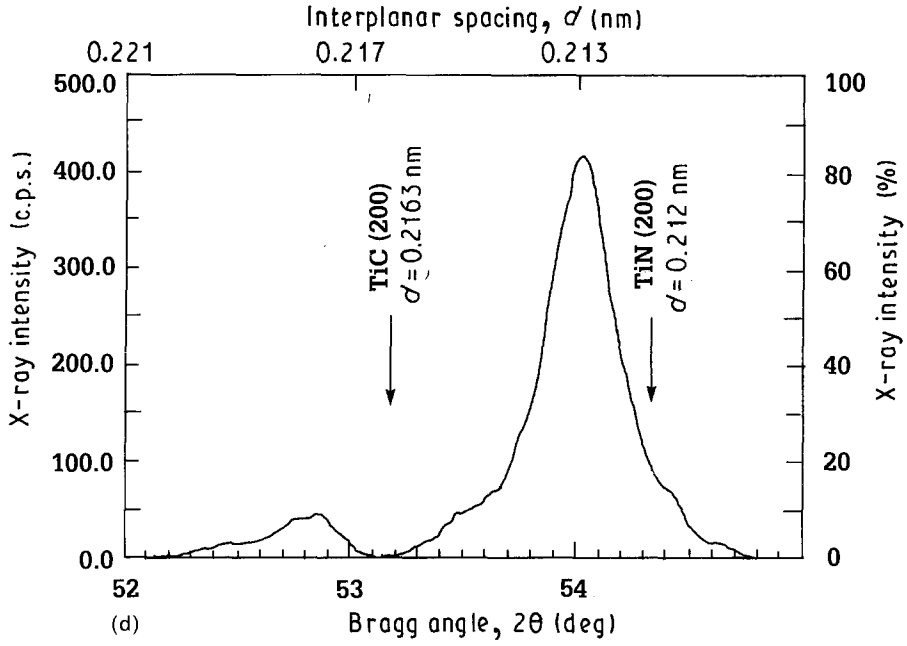

Figure 4 (Contd.)

in going from the substrate to the surface. However, unlike the CVD-SN sample, the Si appears to substitute for Ti on a 1:1 basis. Also, no pure TiN layer is evident. As in all samples examined, a Ti(C, N, O) material is present near the surface. The interlayer on the HPSN sample treated at $H_2/TiCl_4 = 100$ (see Fig. 6b) has a total thickness of 1.8 μm. It consists of three distinct layers, each of approximately uniform composition. The outer layer contains Ti, C, N and O. The middle layer consists of Ti, Si and N, and the inner layer is TiN. Also, a small amount of Si is present on the surface and in the TiN layer. The composition of the $Ti_xSi_yN_z$ layer is close to Ti_5Si_3, with a small excess of Si and a trace amount of N (roughly 5% of the Ti present). This composition was determined by comparison with a standard made from 99.5% pure Ti_5Si_3 powder from AESAR*. An XRD analysis of this layer indicated that it is amorphous or extremely fine-grained.

A skin of Ti(C,N,O) was observed on the surface of all samples examined with the SAM technique. This is believed to be a background contaminant.

A comparison of the SAM results indicates that the total thickness of the interlayer is dependent on the $H_2/TiCl_4$ ratio, with the thickness increasing as the ratio increases. This trend is independent of substrate. Furthermore, at a given $H_2/TiCl_4$ ratio, the interlayer thickness is greater on HPSN than on CVD-SN. This behaviour is consistent with the predictions from thermodynamic modelling. For example, as the $H_2/TiCl_4$ ratio increases, the yield of TiN from $TiCl_4$ is predicted to go up for CVD-SN (see Fig. 2). Note that the Ti/N ratio in the starting material decreases as the $H_2/TiCl_4$ ratio increases. This suggests that, as

*AESAR, Johnson Matthey, 892 Lafayette Road, P.O. Box 1089, Seabrook, NH 03874, USA.

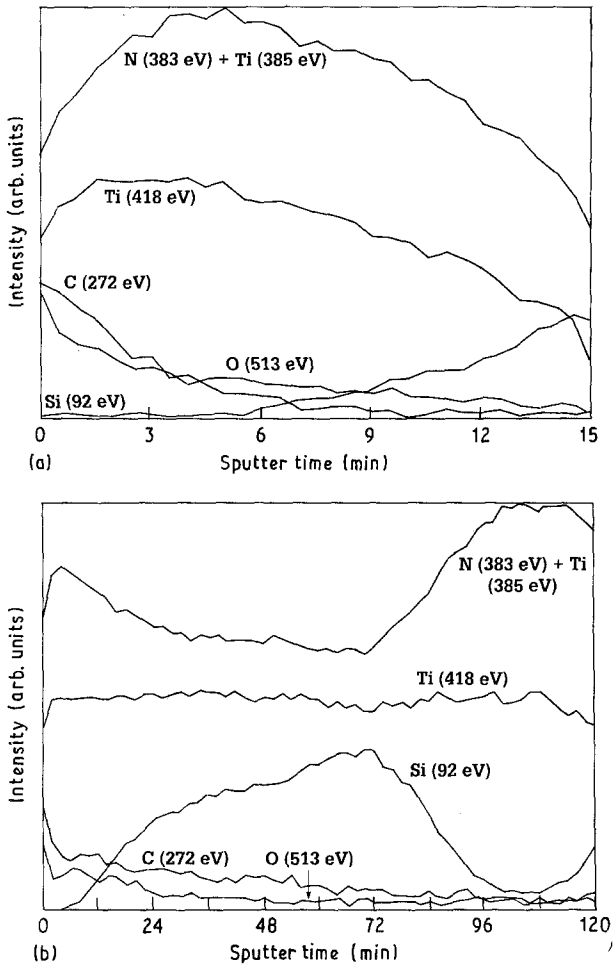

Figure 5 Scanning Auger multiprobe depth profile of interlayer-coated CVD-SN. The sputtering rate was approximately 10 nm min^{-1}. (a) $H_2/TiCl_4 = 5$, (b) $H_2/TiCl_4 = 100$.

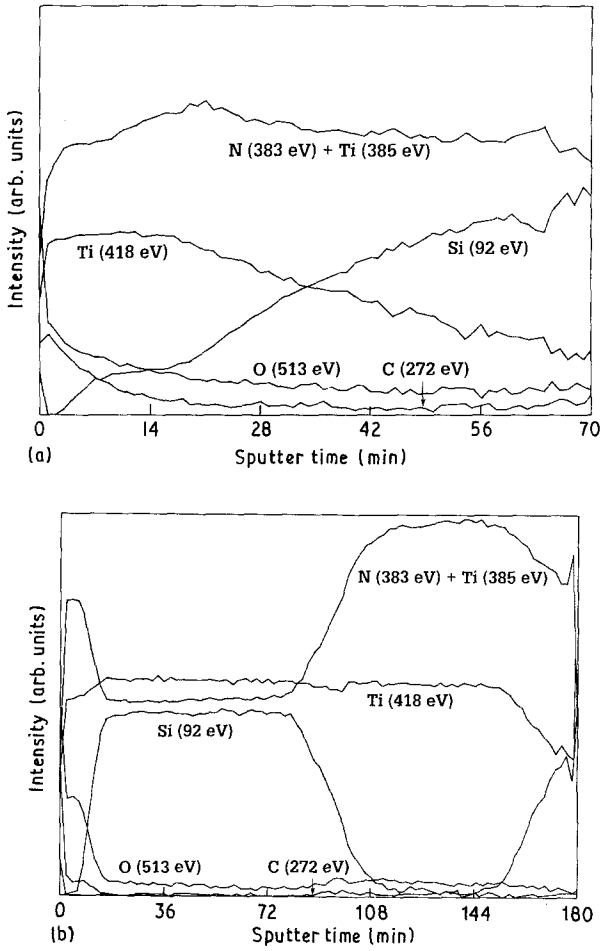

Figure 6 Scanning Auger multiprobe depth profile of interlayer-coated HPSN. The sputtering rate was approximately 10 nm min^{-1}. (a) $H_2/TiCl_4 = 5$, (b) $H_2/TiCl_4 = 100$.

the value of $H_2/TiCl_4$ increases, a thicker TiN film should form for a constant treatment time. At $H_2/TiCl_4 = 100$ for the CVD-SN substrate, solid Si is predicted to form in the interlayer (see Table III). A comparison with the SAM results shows that Si is present in the interlayer on this sample, although it is apparently bonded to Ti. The thermodynamic modelling also predicted less decomposition of the Si_3N_4 initially present in the substrate for CVD-SN than for HPSN due to absence of oxide additives (see Fig. 3). This in turn makes less nitrogen available for reaction with titanium, which translates into less formation of TiN. The SAM results are consistent with this prediction, since the thickness of the TiN layer is smaller on CVD-SN than on HPSN for both of the $H_2/TiCl_4$ ratios studied.

It is of interest to note that studies of interaction between Si_3N_4 and sputter-deposited titanium films have shown that, when these films are heated to temperatures $\geqslant 1000\,^{\circ}C$, TiN forms [13, 14]. Kagawa [13] showed that, on a reaction-bonded Si_3N_4 (RBSN) substrate, interaction between the film and the substrate could lead to the formation of TiN, TiSi or $TiSi_2$. Nobugai *et al.* [14] deposited a Ti-doped amorphous Si_3N_4 film by r.f. sputtering. When heated to temperatures above 1100 °C, precipitates of TiN were formed and the amorphous Si_3N_4 was converted to β-Si_3N_4. Thus, the formation of TiN and/or Ti–Si phases due to a reaction between Ti and Si_3N_4 is not uncommon. The lack of prediction of Ti–Si phases by the thermodynamic model suggests that the reaction is kinetically controlled.

3.3. Machining tests

The effect of the interlayer on machining performance was evaluated by conducting steel turning tests using the parameters listed in Table II. These tests were done on HPSN and HPSNT tools that were uncoated, coated with TiC, TiN, or TiC + Al_2O_3 without the interlayer, and coated with the interlayer and TiC, TiN, or TiC + Al_2O_3. The three outer coating layers – TiC, TiN, or TiC + Al_2O_3– were chosen because they are commonly applied to cutting tools that are used for steel machining.

The various coatings, including the interlayer, were deposited primarily to illustrate the effect of the interlayer on the adhesion and machining performance of subsequent coatings on Si_3N_4. As a result, no attempt was made to optimize the coating thicknesses or CVD process parameters. However, the thicknesses of individual coatings were similar in the two sets of samples (i.e. with and without the interlayer). Since the coating thicknesses were not optimized, the specific tool life is of less significance for this study than the relative tool life. Therefore, the life of uncoated tools was taken as

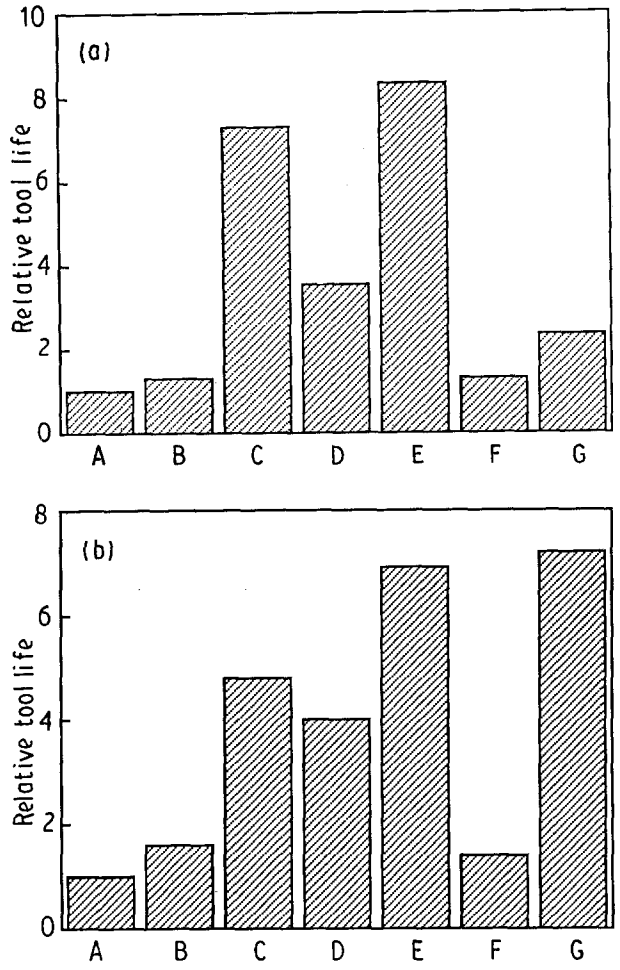

Figure 7 Relative tool life of coated HPSN tools in the machining of 4340 steel: cutting speed (a) 152 m min^{-1}, (b) 213 m min^{-1}. Coating: (A) none, (B) TiC, (C) interlayer + TiC, (D) TiN, (E) interlayer + TiN, (F) TiC + Al_2O_3, (G) interlayer + TiC + Al_2O_3. The results are normalized with respect to the life of an uncoated tool. The principal failure mechanism for all tools was crater wear.

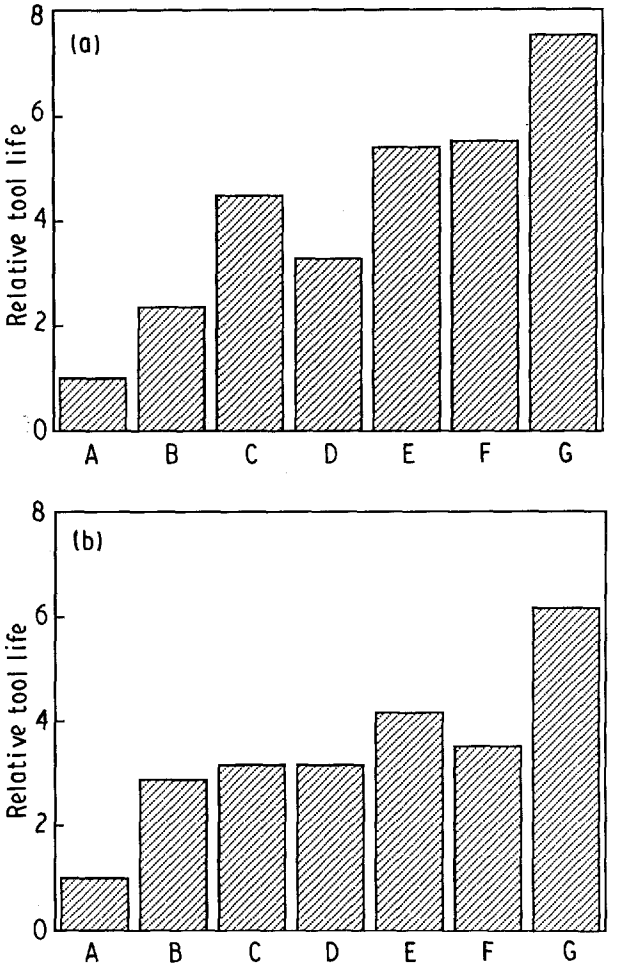

Figure 8 Relative tool life of coated HPSNT tools in the machining of 4340 steel: cutting speed (a) 152 m min^{-1}, (b) 213 m min^{-1}. Coating: (A) none, (B) TiC, (C) interlayer + TiC, (D) TiN, (E) interlayer + TiN, (F) TiC + Al_2O_3, (G) interlayer + TiC + Al_2O_3. The results are normalized with respect to the life of an uncoated tool. The principal failure mechanism for all tools was crater wear.

unity, and the values for coated tools were normalized against those for the uncoated tool.

The normalized results are shown in Figs 7 and 8. In all cases, the coated tools outperformed the uncoated tools. Furthermore, the interlayer gave increased tool life for all coated tools. After the machining tests, each tool was examined by SEM to determine the failure mode. For all tools, the primary failure mode was cratering. As mentioned in section 1, the formation of long, continuous chips in the turning of steel results in a prolonged contact of the chips with the rake face of the tool. The combination of friction, heat, and the chemical affinity of iron with Si_3N_4 in the ambient environment causes a rapid, chemically-enhanced erosion of the tool surface in the contact zone of the chip. This causes a progressive increase in the tool force and decrease in the strength of the cutting edge, eventually resulting in formation of a crater. This type of wear, referred to as chemical wear, was also observed on Si_3N_4 tools in a study of reactivity of iron with various tool materials [2]. In contrast, abrasive wear is the primary wear mechanism in the machining of cast iron. In addition to crater formation, coated tools that had no interlayer showed spalling of the coating beyond the crater, while those with the interlayer showed coating removal only inside the crater. The results for HPSN and HPSNT will be discussed separately.

3.3.1. HPSN

The uncoated tool failed during the first pass, resulting in the formation of a large crater. The size of the crater on HPSN tested at 152 m min^{-1} is shown in Fig. 9a. Application of a coating gave increased tool life, as illustrated in Figs 7 and 8, and this coincided with a reduced crater size even though the tool was tested for a larger number of passes. Furthermore, the crater size was reduced even further when the interlayer was present on coated tools. The reduction in crater size is illustrated in Fig. 9b–e for coated tools with and without the interlayer. These tools were tested at 152 m min^{-1}, but similar results were obtained for tools tested at 213 m min^{-1}. The increased tool life and reduced crater size also coincided with a larger critical load for coating failure during scratch testing [15].

The effect of the interlayer on coating adhesion is illustrated further in Fig. 10, where coating damage near the cutting edge is shown in detail. Fig. 10a shows

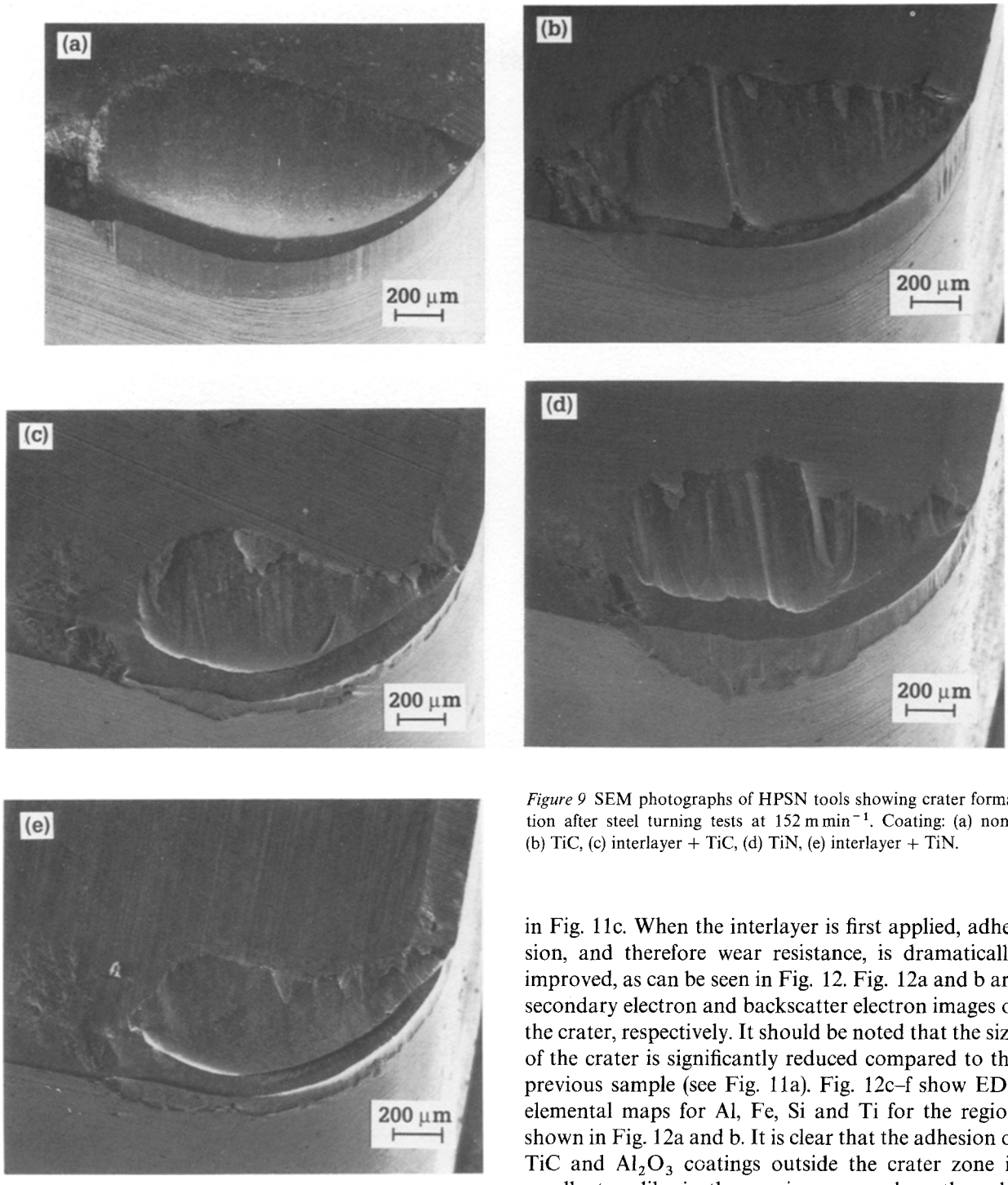

Figure 9 SEM photographs of HPSN tools showing crater formation after steel turning tests at 152 m min^{-1}. Coating: (a) none, (b) TiC, (c) interlayer + TiC, (d) TiN, (e) interlayer + TiN.

the edge of the crater on TiC-coated HPSN. The coating has spalled off from a region approximately 20 μm beyond the crater edge. In contrast, no spalling occurred on the (interlayer + TiC)-coated HPSN tool (Fig. 10b). The light-coloured regions on the crater surfaces are iron from the steel that adhered to the tool. Similar results were obtained for TiN-coated and (interlayer + TiN)-coated HPSN, as illustrated in Fig. 10c and d, respectively. Results for (TiC + Al_2O_3)-coated HPSN were also similar.

When no interlayer is present, the coating has spalled down to the substrate, as shown in Fig. 11. Fig. 11a shows the crater size, and Fig. 11b shows exposed substrate beyond the crater edge. This is further illustrated by the Si energy-dispersive spectrometry (EDS) elemental map of the crater zone shown in Fig. 11c. When the interlayer is first applied, adhesion, and therefore wear resistance, is dramatically improved, as can be seen in Fig. 12. Fig. 12a and b are secondary electron and backscatter electron images of the crater, respectively. It should be noted that the size of the crater is significantly reduced compared to the previous sample (see Fig. 11a). Fig. 12c–f show EDS elemental maps for Al, Fe, Si and Ti for the region shown in Fig. 12a and b. It is clear that the adhesion of TiC and Al_2O_3 coatings outside the crater zone is excellent, unlike in the previous case where the substrate was exposed well beyond the crater area.

3.3.2. HPSNT

As with HPSN, the uncoated tool failed during the first pass and showed a large crater (Fig. 13a). The effects of TiC and TiN coatings with and without the interlayer on crater size are illustrated in Fig. 13b–e for tools tested at 152 m min^{-1}. Notice the spalling of the TiC coating beyond the crater in Fig. 13b. Similar results were also obtained for tools tested at 213 m min^{-1}.

When a TiC + Al_2O_3 coating is present, the coating has spalled down to the substrate (Fig. 14a–d). Comparison of the Si EDS elemental map of the crater zone (Fig. 14b) with the crater shown in Fig. 14a shows exposed substrate beyond the crater boundary.

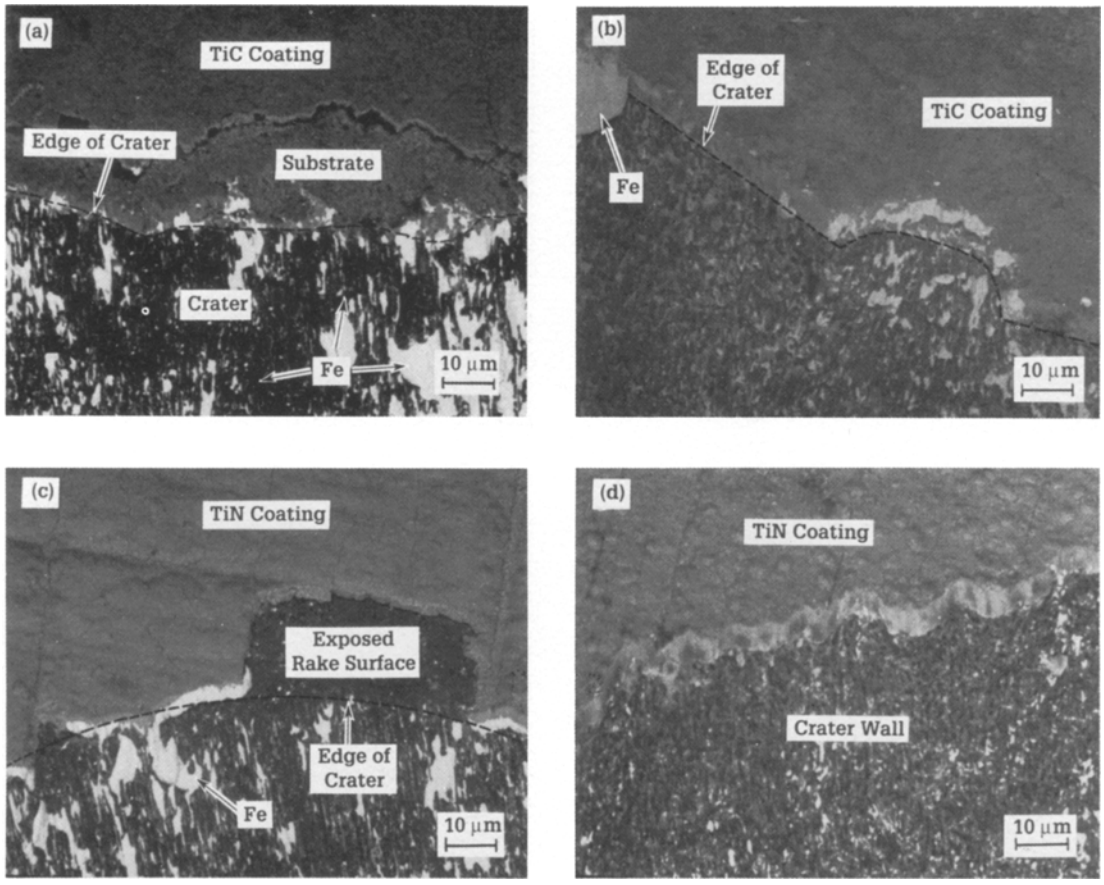

Figure 10 SEM photographs of coated HPSN tools showing effect of interlayer on coating adhesion after steel turning tests at 152 m min^{-1}: (a) edge of crater in TiC-coated tool showing loss of coating adhesion on the rake face, (b) edge of crater in (interlayer + TiC)-coated tool showing good coating adhesion, (c) edge of crater in TiN-coated tool showing loss of coating adhesion on the rake face, (d) edge of crater in (interlayer + TiN)-coated tool showing good coating adhesion.

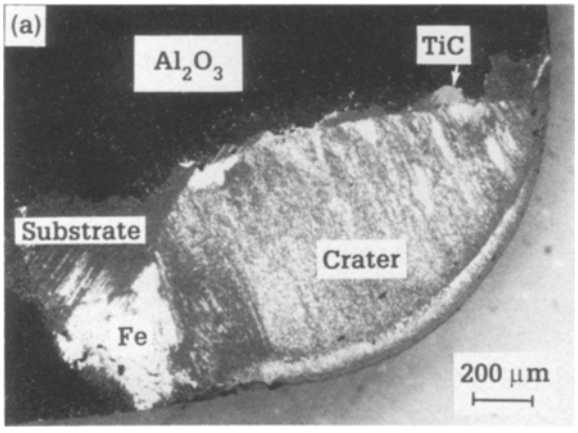

The Al EDS elemental map (Fig. 14c) shows that the Al_2O_3 coating is completely removed in the crater region. However, fragments of the TiC coating remain just beyond the crater edge (Fig. 14d). This is indicative of strong adherence of the TiC layer to the substrate, which may be due to the presence of TiC particles in the substrate as discussed in section 3.2.1. Similar TiC coating fragments were not found on (TiC

Figure 11 SEM photographs of (TiC + Al_2O_3)-coated HPSN tools without the interlayer after steel turning tests at 152 m min^{-1}: (a) secondary electron image of crater zone showing spalling of coating beyond the crater, (b) backscattered electron image of area in (a), (c) Si dot map (EDS) of area in (a) showing complete removal of coating from the crater zone, beyond the wear area.

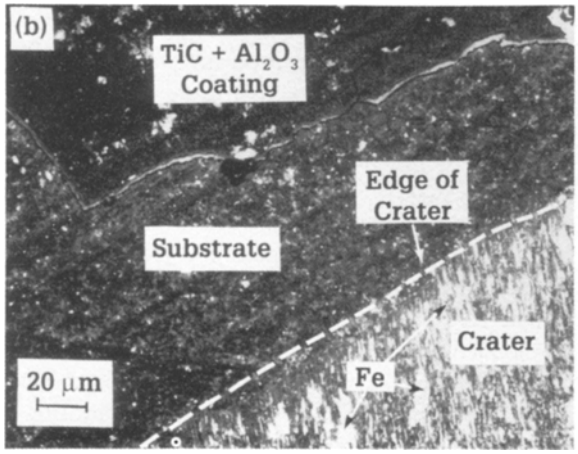

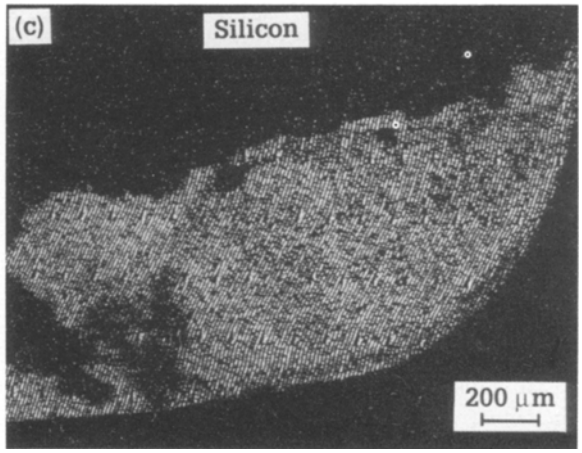

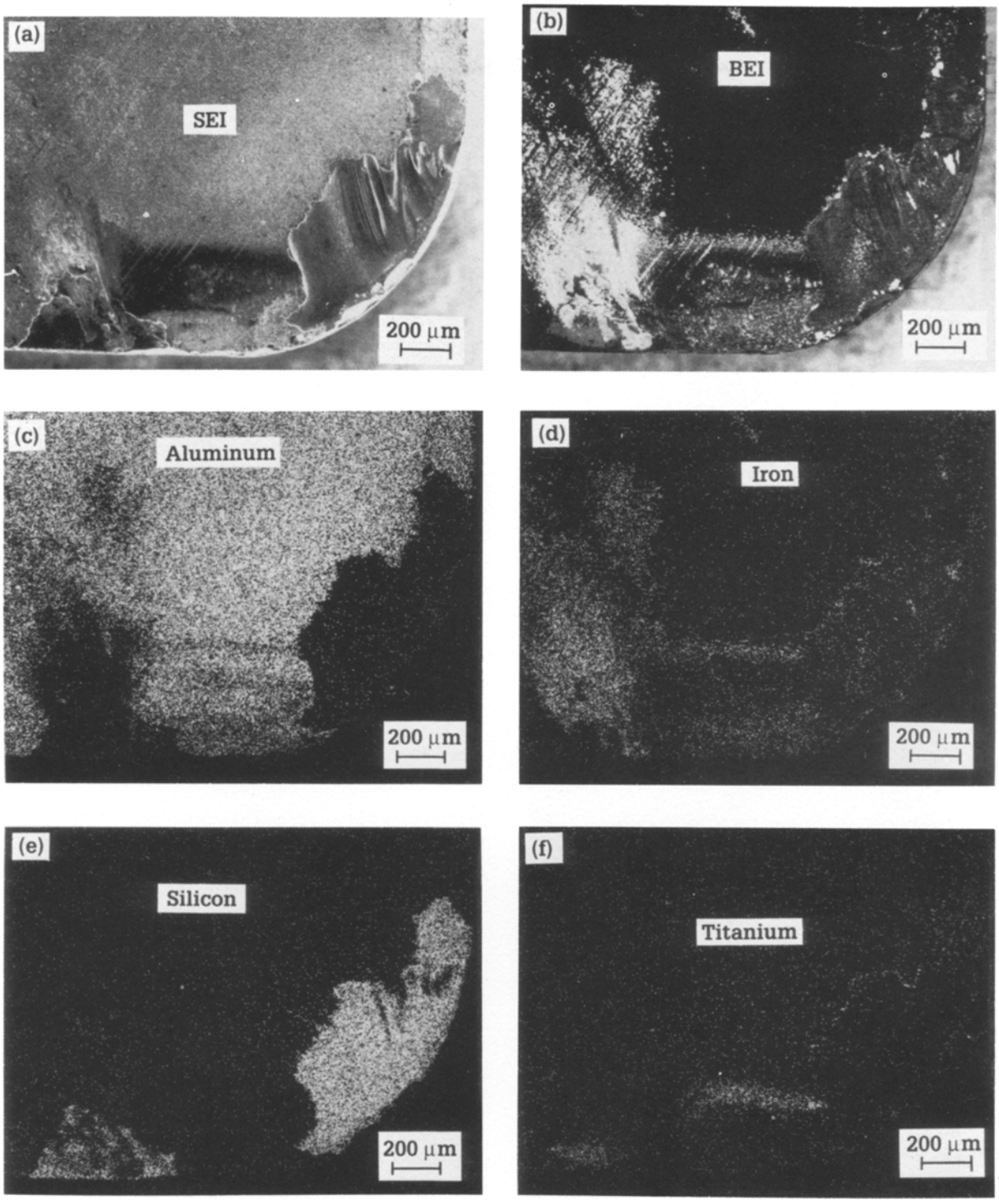

Figure 12 SEM photographs of (TiC + Al_2O_3)-coated HPSN with interlayer after steel turning tests at 152 m min^{-1}: (a) secondary electron image of crater zone showing a much smaller crater size, (b) backscattered electron image of the same area, (c) Al dot map (EDS) of wear area showing retention of coating beyond the crater, (d) Fe dot map showing remnants of chips adhering to the tool, (e) Si dot map showing removal of coating from the crater area, (f) Ti dot map showing spots where Al_2O_3 coating has been removed. This shows that the adhesion between TiC and the substrate is excellent. Compare with Fig. 11.

+ Al_2O_3)-coated HPSN, which contains no TiC in the substrate. The enhanced adhesion of the TiC coating on HPSNT coincided with improved machining performance relative to the uncoated substrate when compared to HPSN (compare Figs 7 and 8).

Similar results were obtained by Kim *et al.* [16], who observed a distinct interface in a TiC-coated Si_3N_4 + TiC composite similar to HPSNT. They found a 1.3 μm thick interface in the TiC-coated sample. In contrast, a 0.6 μm interface was found in a TiN-coated sample. The improved performance of TiC-coated tools relative to TiN-coated tools was attributed to this interface, suggesting that the adhesion of the TiC coating to the substrate was better than that of the TiN coating. Interestingly, these authors did not observe any reaction between the TiC particles in the substrate and the TiN coating. As shown in Fig. 4d, the formation of the interlayer on

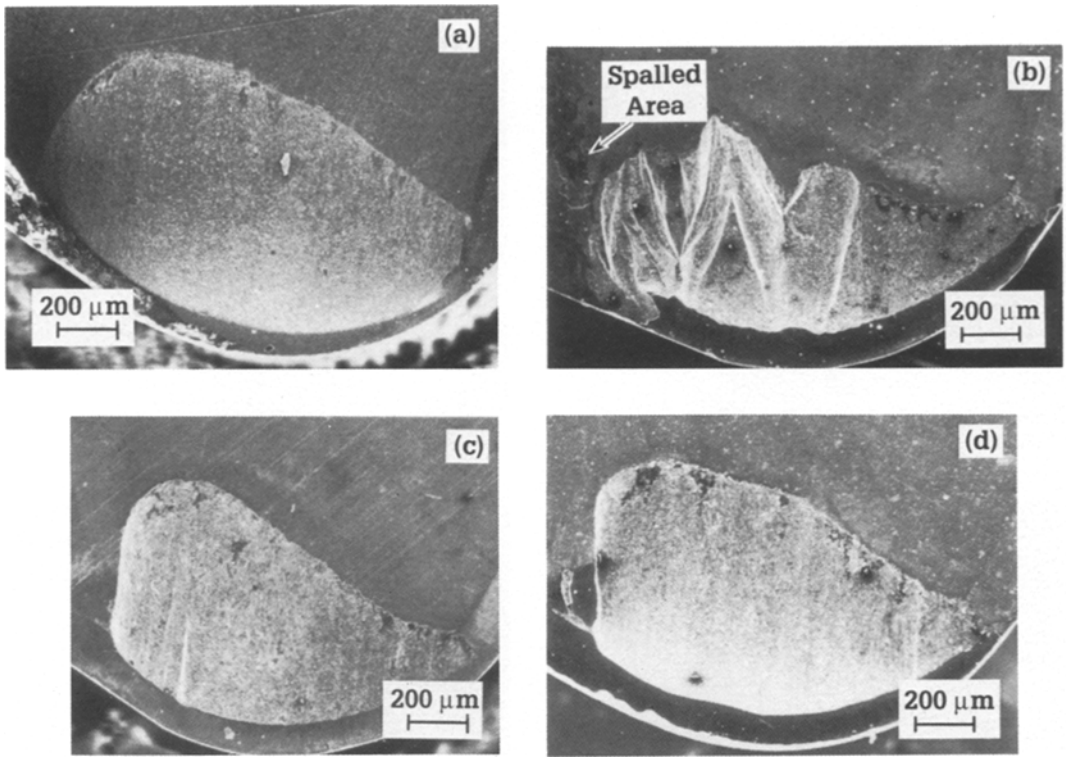

Figure 13 SEM photographs of HPSNT tools showing crater formation after steel turning tests at 152 m min^{-1}: (a) uncoated HPSNT, (b) TiC-coated HPSNT, (c) (interlayer + TiC)-coated HPSNT, (d) TiN-coated HPSNT, (e) (interlayer + TiN)-coated HPSNT.

HPSNT resulted in a Ti(C, N) phase in this work. Thus, the formation of a TiN film on HPSNT produced a diffusion interface incorporating the dispersed and second phase in the substrate, thereby further enhancing the adhesion of subsequent coatings. The

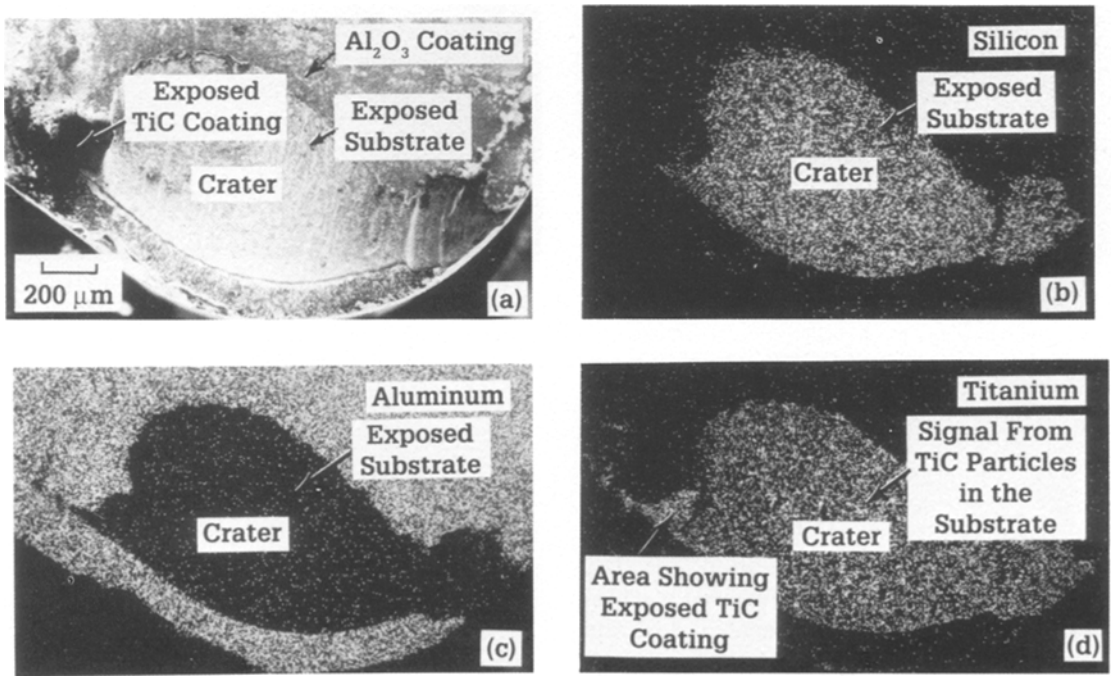

Figure 14 SEM photographs of (TiC + Al_2O_3)-coated HPSNT tools without interlayer after steel turning tests at 152 m min^{-1}: (a) crater region showing spalling of the coating beyond the crater area, (b) Si dot map (EDS) of wear area showing removal of coating from the crater area, (c) Al dot map of wear area showing complete removal of Al_2O_3 coating, (d) Ti dot map of wear area showing spots where Al_2O_3 coating has been removed.

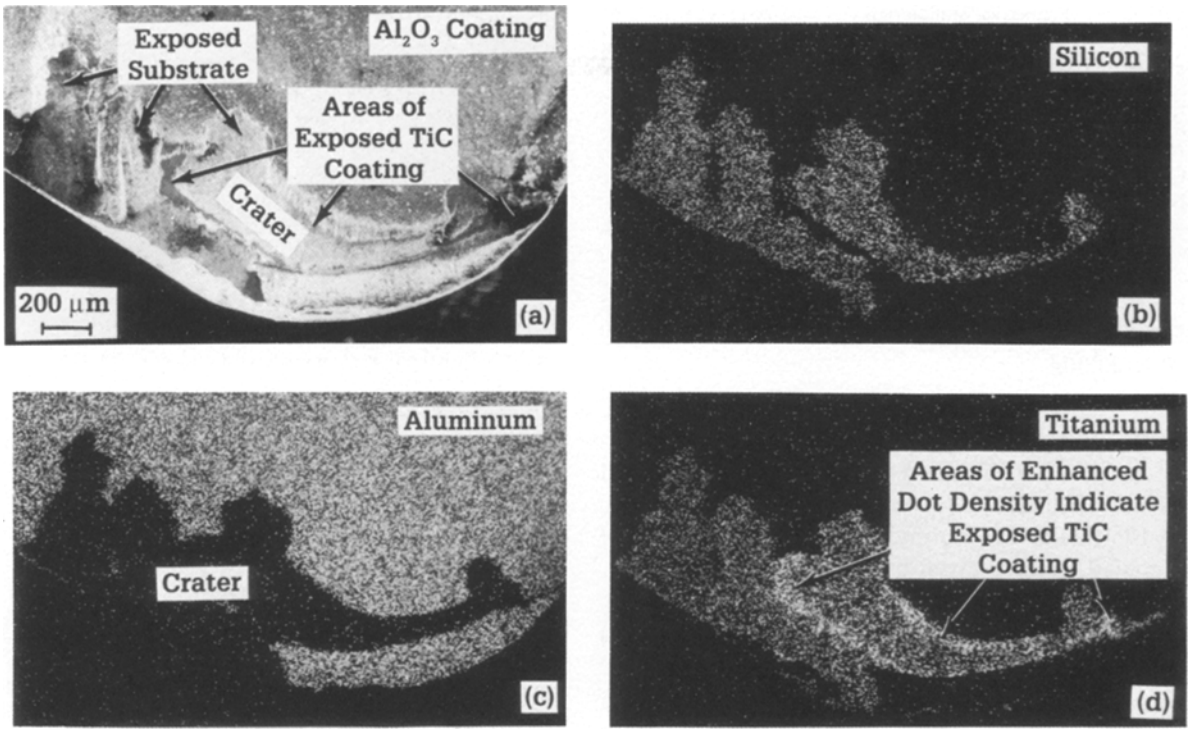

Figure 15 SEM photographs of (TiC + Al_2O_3)-coated HPSNT tools with interlayer after steel turning tests at 152 m min^{-1} (a) crater region showing a smaller crater size, (b) Si dot map (EDS) of wear area showing removal of coating from the crater area, (c) Al dot map of wear area showing complete removal of Al_2O_3 coating, (d) Ti dot map of wear area showing spots where Al_2O_3 coating has been removed. Compare with Fig. 14.

survival of TiC coating fragments beyond the crater in the machine-tested (TiC + Al_2O_3)-coated HPSNT sample (Fig. 14d) underscores the beneficial effect of the diffusion interface.

Application of the interlayer to (TiC + Al_2O_3)-coated HPSNT gave an improvement in tool life relative to the tool without the interlayer, as illustrated by the reduced crater size shown in Fig. 15a relative to that in Fig. 14a. However, regions of exposed substrate still formed beyond the crater, as shown by the Si EDS elemental dot map in Fig. 15b. This is similar to the behaviour observed for the (TiC + Al_2O_3)-coated HPSNT tool without the interlayer. Also, the Al_2O_3 coating is completely removed in the crater region (Fig. 15c), but fragments of the TiC coating remain (Fig. 15d).

4. Summary and conclusions

This study showed that the application of TiC, TiN and TiC + Al_2O_3 coatings to Si_3N_4-based cutting tool inserts improves tool life in steel turning applications. However, when these coated tools fail, it is often due to loss of adhesion of the coating from the substrate. It was shown that this problem can be overcome by applying an interlayer between the coating and the substrate. The interlayer is produced by chemically reacting $TiCl_4$ with the substrate at high temperature, using a chemical vapour deposition process similar to that used to deposit the coatings. Thermodynamic modelling of the interlayer deposition process was done, and it predicted that a TiN layer should form on the surface of the substrate during the interlayer deposition process. Analysis of the interlayer using X-ray diffraction and a scanning Auger microprobe confirmed the presence of TiN. Steel turning tests of tools coated with and without the interlayer showed substantial improvement in the tool life when the interlayer was present.

Acknowledgements

The authors wish to thank the managements of GTE Laboratories and GTE Valenite for permission to publish this work. We are also indebted to Mark Jagner, Dhiraj Shah and Gary Pylar of the Materials Characterization Laboratory of GTE Valenite for their help, enthusiasm and interest in the analysis of samples. We also thank Prasad Boppana of GTE Valenite for his help in conducting the machining tests and in the analysis of tool failure, and John Roman of GTE Valenite for coating the samples.

Appendix

The stress due to a mismatch of thermal expansion coefficients between a coating and a substrate, in the absence of plastic deformation, is given by [17]

$$\sigma_T = \frac{E_s E_c \Delta T(\alpha_s - \alpha_c)}{E_s + 2E_c(t_c/t_s)} \quad \text{(A1)}$$

where σ_T = tangential stress in the coating; E_s, E_c = elastic moduli of substrate and coating, respectively; ΔT = temperature change from deposition temperature; α_s, α_c = coefficients of thermal expansion (CTE) for substrate and coating, respectively and

TABLE A1 Properties of materials

Material	CTE ($K^{-1} \times 10^{-6}$)	E(GPa)	Ref.
Si_3N_4 with 3.5 wt % MgO	3.24	–	18
TiC	8.6	430	19
TiN	8.0	215	19

t_c, t_s = thicknesses of coating and substrate, respectively. The expression can be simplified for a case where $t_c \ll t_s$, giving

$$\sigma_T = E_c \Delta T(\alpha_s - \alpha_c) \quad \text{(A2)}$$

The required physical properties of the various materials are given in Table A1. With these values and $\Delta T = -1000$ K, $\sigma_{T,TiC} = 2.305$ GPa and $\sigma_{T,TiN} = 1.1950$ GPa. The normal stress at a sharp edge of the coated insert is given by [17]

$$\sigma_N = E_c \Delta T\left(\frac{t_c}{r}\right)(\alpha_s - \alpha_c) \quad \text{(A3)}$$

where r is the radius of curvature at the edge. For a TiC coating of 5 μm on a Si_3N_4 substrate with a radius of curvature at the cutting edge of 50 μm, Equation A3 gives $\sigma_{N,TiC} = 0.230$ GPa. For a TiN coating of the same thickness on the same substrate, $\sigma_{N,TiN} = 0.120$ GPa.

References

1. M. FUKUHARA, K. FUKUZAWA and A. FUKAWA, *Wear* **102** (1985) 195.
2. J. G. BALDONI and S.-T. BULJAN, *Ceram. Bull.* **67**(2) (1988) 381.
3. S. J. BURDEN, US Patent 4 652 276 (1987).
4. A. EZIS, S. K. SAMANTA and K. SUBRAMANIAN, US Patent 4 434 238 (1984).
5. M. FURUKAWA, K. MISUMI, Y. TAKANO and M. NAGANO, *Nippon Tungsten Rev.* **15** (1982) 1.
6. V. K. SARIN and S.-T. BULJAN, US Patent 4 449 989 (1984).
7. V. K. SARIN, S.-T. BULJAN and C. D'ANGELO, US Patent 4 409 004 (1983).
8. *Idem*, US Patent 4 416 670 (1983).
9. P. A. STEINMANN, Y. TARDY and H. E. HINTERMANN, *Thin Solid Films* **154** (1987) 333.
10. D. G. BHAT, D. C. SHAH, J. R. KYLE and P. F. WOERNER, US Patent 4 640 693 (1987).
11. D. G. BHAT, P. F. WOERNER and V. K. SARIN, US Patent 4 670 024 (1987).
12. S. GORDON and B. J. McBRIDE, "Computer program for calculation of complex chemical equilibrium compositions, rocket performance, incident and reflected shocks, and Chapman-Jouguet detonations", NASA Report SP-273 (NASA, Washington, DC 1976).
13. Y. KAGAWA, *J. Mater. Sci. Lett.* **4** (1985) 1062.
14. K. NOBUGAI, S. YABE and F. KANAMARU, *J. Amer. Ceram. Soc.* **67**(7) (1984) C-143.
15. H. E. REBENNE, D. G. BHAT and P. F. WOERNER, in Proceedings of 3rd International Conference on Surface Modification, edited by T. S. Sudarshan and D. G. Bhat (Metallurgical Society, Warrendale, PA, 1990) p. 261.
16. D. W. KIM, Y. J. PARK, J. G. LEE and J. S. CHUN, *Thin Solid Films* **165** (1988) 149.
17. C. F. POWELL, in "Vapor Deposition", edited by C. F. Powell, J. H. Oxley and J. N. Blocher (Wiley, New York, 1966) p. 198.
18. R. M. WILLIAMS, *J. Amer. Ceram. Soc.* **63**(1/2) (1980) 108.
19. W. J. LACKEY, D. P. STINTON, G. A. CERNY, A. C. SCHAFFHAUSER and L. L. FEHRENBACHER, *Advanced Ceram. Mater.* **2**(1) (1987) 24.

Received 19 April
and accepted 30 November 1990